Radiometric compensation for cooperative distributed multi-projection system through 2-DOF distributed control.

AUTHOR(S):

Tsukamoto, Jun; Iwai, Daisuke; Kashima, Kenji

CITATION:

Tsukamoto, Jun ...[et al]. Radiometric compensation for cooperative distributed multi-projection system through 2-DOF distributed control.. IEEE transactions on visualization and computer graphics 2015, 21(11): 1221-1229

ISSUE DATE:

2015-11-15

URL:

http://hdl.handle.net/2433/203058

Radiometric Compensation for Cooperative Distributed Multi-Projection System through 2-DOF Distributed Control

Jun Tsukamoto, Daisuke Iwai, and Kenji Kashima, *Member, IEEE*

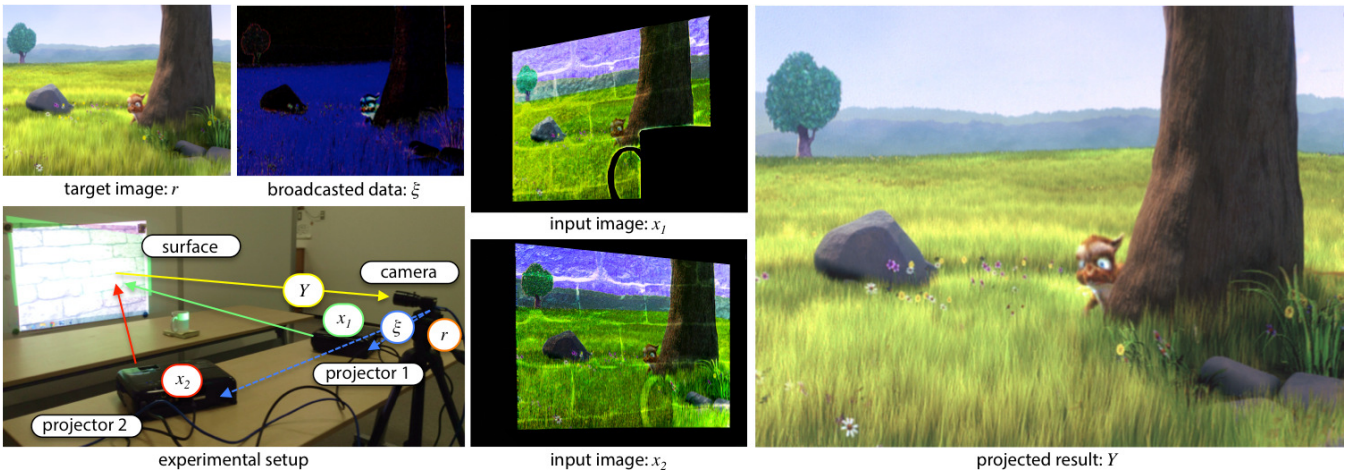

Fig. 1. A projected result Y of the proposed radiometric compensation technique based on 2-DOF distributed control for the 76-th frame of the anial movie (see Section 5). To make the system scalable, a broadcasting from the camera node to the projector nodes was only used as a communication method. Therefore, the input image to each projector x_i was computed on each projector node using a broadcasted data ξ from the camera node, which was computed with target image r and the previous projected result. Note that some areas in the input images are masked for better visibility, where artifacts occur due to geometric calibration errors, which do not affect the projected result at all.

Abstract—This paper proposes a novel radiometric compensation technique for cooperative projection system based-on distributed optimization. To achieve high scalability and robustness, we assume cooperative projection environments such that 1. each projector does not have information about other projectors as well as target images, 2. the camera does not have information about the projectors either, while having the target images, and 3. only a broadcast communication from the camera to the projectors is allowed to suppress the data transfer bandwidth. To this end, we first investigate a distributed optimization based feedback mechanism that is suitable for the required decentralized information processing environment. Next, we show that this mechanism works well for still image projection, however not necessary for moving images due to the lack of dynamic responsiveness. To overcome this issue, we propose to implement an additional feedforward mechanism. Such a 2 Degree Of Freedom (2-DOF) control structure is well-known in control engineering community as a typical method to enhance not only disturbance rejection but also reference tracking capability, simultaneously. We theoretically guarantee and experimentally demonstrate that this 2-DOF structure yields the moving image projection accuracy that is overwhelming the best achievable performance only by the distributed optimization mechanisms.

Index Terms—Projector-camera system, radiometric compensation, distributed optimization, control theory

1 Introduction

Radiometric compensation is an important fundamental technology for projection-based augmented reality (AR), which corrects color artifacts of projected imagery on textured surfaces [7]. It has expanded the application fields of projection-based AR by allowing not only surfaces suitable for projections, such as uniformly white objects, but almost arbitrary diffuse surfaces even with textures, to be projection targets. So far, much effort has been put on improving compensation accuracy for a single projection system. However, due to various factors such as the limited dynamic ranges of projectors and shadows of projected images, a single projection is not sufficient to provide acceptable projection results in many application scenarios. In this paper, we focus on radiometric compensation for a cooperative overlapping multi-projection system that has several advantages over a single projection system, such as higher maximum luminance while covering wider field of view and less shadows.

There are several technical issues for radiometric compensation of a cooperative multi-projection system, which are not necessarily considered in the previous researches for a single projection system. For example, the system should be scalable so that it accommodates the demand of increasing computational costs and communications traffic when the number of projector nodes increases. In other words, it is important to have a Plug-and-Play capability by which a newly added (plug-in) projector node is automatically connected to the system's network. The system also should be robust for the failure (plug-out) of projector nodes at runtime. However, these issues have not been

- *Jun Tsukamoto is with Kyoto University. E-mail: tsukamoto.jun.64a@st.kyoto-u.ac.jp.*
- *Daisuke Iwai is with Osaka University. E-mail: daisuke.iwai@sys.es.osaka-u.ac.jp.*
- *Kenji Kashima is with Kyoto University. E-mail: kashima@amp.i.kyoto-u.ac.jp.*

carefully considered in the radiometric compensation research field.

To achieve high scalability, robustness and Plug-and-Play capability as mentioned above, we propose to apply a distributed optimization algorithm based on distributed control theory to radiometric compensation for a cooperative overlapping projection system, rather than a centralized control approach in which a host node computes projection images for all projector nodes. Unique properties of our distributed projection system consisting of a camera node and multiple projector nodes are: (1) each projector node does not have any information about other projector nodes as well as target images, (2) the camera node does not have any information about the projector nodes either, while having the target images, and (3) only a broadcast communication from the camera node to the projector nodes is allowed to suppress the data transfer bandwidth. A preliminary result suggests that a distributed optimization algorithm based on feedback control potentially works for the radiometric compensation in our distributed projection system [20]. However, it practically requires tens of frames to converge, and consequently, works only for displaying static images.

In this paper, we propose a novel radiometric compensation technique for our distributed projection system by combining the previously proposed distributed optimization with centralized feedforward mechanism while preserving the distributed feedback structure. The new technique improves the tracking responsiveness (i.e., speed of convergence) to realize the projections of radiometrically compensated moving images. Based on a control theoretic approach, we evaluate the improvement through the comparison of error-to-reference ratios in the frequency domain between the previous feedback-only and the proposed 2 degree of freedom (DOF) (i.e., feedback and feedforward) control designs. We also conduct real projection experiments to validate moving image qualities of compensated results.

To summarize, this paper makes the following contributions:

- We provide the theoretical performance limit of a distributed optimization algorithm based on a feedback control for radiometric compensation in terms of the tracking responsiveness using a control theoretic approach.
- We combine centralized feedforward mechanism with the distributed optimization structure for improving the tracking responsiveness to realize radiometric compensation of moving images.
- Through real projection experiments, we show the feasibility of the proposed method for moving images, in terms of the compensation accuracy and the speed of convergence.

2 Related Work

Radiometric compensation has been an active research topic in projection-based AR. Most radiometric compensation techniques apply a projector-camera system (procams) to compensate for projected colors disturbed by textures on projection surfaces. Bimber et al. proposed a simple linear model to describe the relationship between an input pixel value to the projector of a procams and projected result captured by a corresponding camera pixel [6]. Using the model, they computed an input image for the projector to display a target image on arbitrary textured Lambertian surfaces. More complex but accurate models have been also proposed, such as one that considers the crosstalk of color channels [23] and another that considers color valuation within a projector pixel area [14].

These compensation methods assume single projection systems. On the other hand, multi-projection systems are desirable in many application scenarios of projection-based AR, because they solve various inherent problems of single projection approach such as limited maximum intensity, defocus blur, and cast shadow [5, 15, 12]. Researchers also tried to solve the radiometric compensation issue in multi-projection systems. Bimber et al. applied their method to a multi-projection system by evenly dividing target colors to all projectors [6]. Bermano et al. proposed more general method that computes a compensation image using a light transport matrix that describes a relationship between input pixel values for all pixels of all projectors and the projected result [3]. Although these methods worked well, they heavily rely on a host computer that have centralized control over all projectors. Therefore, they are not suitable for our goal that is to realize a highly scalable, robust, and Plug-and-Play capable radiometric compensation, as mentioned in the first section. Recently, it was reported that projected results converged in a multiple overlapping projection system by independently controlling them based on model predictive control theory [1, 2]. However, it was also pointed out that the technique did not accurately display target appearances because of the interference among projections, and it was not designed to display moving images.

In this paper, leveraging the recent rapid sophistication of distributed control theory that is consequently expanding its application fields [13, 8], we build a radiometric compensation technique that meets our requirements (i.e, scalability, robustness, and Plug-and-Play capability) using a distributed optimization algorithm [16]. We theoretically guarantee the convergence of projected results to target appearances by explicitly assuming dynamic interference of multiple overlapping projections on a surface in stability analysis. Furthermore, to improve the speed of convergence of our distributed optimization, we combine a centralized feedforward mechanism to compensate for moving images, while preserving the distributed feedback structure. To the best of our knowledge, this is the first attempt to introduce distributed optimization framework from distributed control theory for radiometric compensation of cooperative multi-projection system.

3 Problem Formulation and Previous Work

This section describes the problem formulation of this researh and previously proposed radiometric compensation algorithm for our distributed projection system [20]. We build our method based on the Bimber's linear model [6]. As with most of radiometric compensation methods, we assume our projection objects as arbitrary shaped and textured but limited to Lambertian surfaces.

3.1 System architecture and problem formulation

We consider a projector-camera system composed of n projector nodes and one camera node that is regarded as an eye of a human observer. Each projector node i has an input image $x_i^j \in [0,1]$ and form factor p_i^j for the j-th pixel. Here, the form factor is the ratio of the projected result image captured by the camera to the input image at each pixel under completely dark environment. This is normally acquired by projecting a uniform white image and capturing the reflection on a projection surface. This value is affected by the reflectance of the surface, the distance between the projector to the surface, incident angle of projected light, and so on. It is necessary to calibrate the form factor of the projector once when it is newly added to the system. In this setting, the camera observation at the j-th pixel can be represented as

$$Y^j = \sum_i p_i^j x_i^j + d^j, \tag{1}$$

where d^j is environmental light (e.g. ambient light and black offset) (Figure 3). The camera node has a target image r^j and importance map ϕ^j at each pixel. Typical examples of the importance map are Saliency map [11] and Threshold map [17, 21]. Symbols of this model are listed in Figure 1.

In order to project the target image accurately, we minimize the objective function

$$G(x) = \frac{1}{2}\sum_j \phi^j (e^j)^2,\ x = (x_i^j),\ i \in \mathscr{L},\ j \in \mathscr{J}, \tag{2}$$

which is the sum of the squared error

$$e^j = r^j - Y^j = r^j - \sum_{i=1}^{n} p_i^j x_i^j - d^j, \tag{3}$$

weighted by the importance map.

$i \in \mathscr{I} := \{1,2,\cdots,n\}$	projector index
$j \in \mathscr{J} := \{1,2,\cdots,m\}$	pixel index
$x_i^j \in [0,1]$	input image
$p_i^j \in \mathbb{R}_+$	form factor
$Y^j \in \mathbb{R}(j \in \mathscr{J})$	projected result image
$r^j \in \mathbb{R}_+(j \in \mathscr{J})$	target image
$d^j \in \mathbb{R}(j \in \mathscr{J})$	environmental light
$\phi^j \in \mathbb{R}_+(j \in \mathscr{J})$	importance map

Fig. 2. Notation.

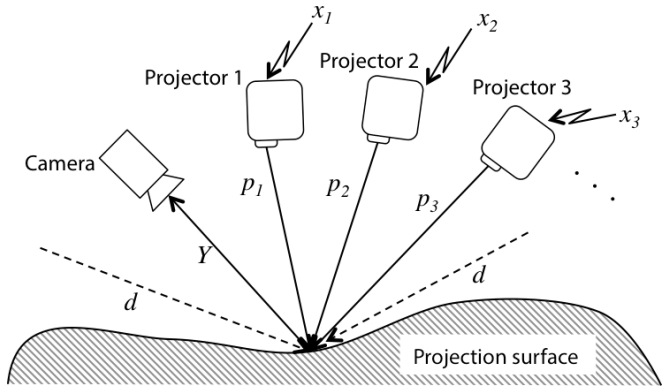

Fig. 3. System architecture.

3.2 Previous result: Distributed feedback algorithm

To achieve high scalability and robustness, we assume that x_i^j and p_i^j are available only for the projector node i, and that r^j, Y^j and ϕ^j are available only for the camera node. Thanks to the specific structure of (2), we can optimize x_i^j in such a distributed setting. The gradient of (2) is given by

$$\frac{\partial G}{\partial x_i^j} = -p_i^j \phi^j e^j. \tag{4}$$

Therefore, if $\phi^j e^j$ is available, each projector node can compute the gradient without any other information about the other projectors. For implementation, the camera node can compute and broadcast

$$\xi^j[k] = K\phi^j e^j[k] = K\phi^j(r^j - Y^j[k]), \tag{5}$$

where K is a positive constant. Then, each projector updates $x_i^j[k]$ by

$$x_i^j[k+1] = \mathscr{P}[x_i^j[k] + \underbrace{p_i^j \xi^j[k]}_{K\frac{\partial G}{\partial x_i^j}[k]}] \tag{6}$$

$$\mathscr{P}[\bar{x}] := \begin{cases} \bar{x}, & 0 \le \bar{x} \le 1, \\ 1, & \bar{x} > 1, \\ 0, & \bar{x} < 0, \end{cases} \qquad \bar{x} \in \mathbb{R}. \tag{7}$$

This algorithm is equivalent to a (projected) gradient method to minimize G where K works as a stepsize. Actually, it can be proven that this update rule with *sufficiently small* K makes x_i^j converge to the optimal value in a suitable sense [19]. As described above, once $\xi^j[k]$ is broadcasted to all the projector nodes from the camera node, the projector nodes can compute input images without other communications among the nodes in the system. This is a completely distributed process, and furthermore, it is theoretically guaranteed that removal or addition of projector nodes at run time does not affect the convergence performance.

Since this algorithm is decoupled pixelwise, the superscript j is omitted hereafter. Further, $\phi_j = 1$ is assumed without loss of generality.

4 Proposed Algorithm

We propose a novel 2-DOF control algorithm that improves the tracking responsiveness of our previously proposed distributed feedback algorithm [20] (see Section 3.2). First, we apply a control theoretic approach to analyze the performance and its limit of the previous method. Second, we describe our new technique that combines a centralized feedforward mechanism with the distributed feedback algorithm. Then, we show the improvement of tracking responsiveness by comparing Frequency dependent error-to-reference ratios.

4.1 Performance limit of the feedback scheme

In [20], the target projection image was assumed to be *static*. Thus, k in the previous section was no more than the iteration index, and r was k-independent. In this paper, we attempt to project *movies*. To formulate this situation, we regard k as (discrete) time or frame number, and the target movie is represented by $r[k]$. Similarly to the previous case, we minimize the error

$$e[k] = r[k] - Y[k]. \tag{8}$$

It is possible to simply replace r in (5) by $r[k]$. However, it should be noted that due to this time-dependency, the responsiveness of the overall system is more important than the previous case. To analyze such a dynamic behavior, it is informative to streamline the resulting system equation without considering the effect of saturation and disturbance d as follows:

$$\begin{aligned} e[k+1] &= r[k+1] - Y[k+1] \\ &= r[k+1] - \left\{ \sum_{i=1}^n p_i x_i[k+1] \right\} \\ &= r[k+1] - \left\{ \sum_{i=1}^n p_i (x_i[k] + K \sum_{i=1}^n p_i e[k]) \right\} \\ &= r[k+1] - \left\{ (r[k] - e[k]) + K \sum_{i=1}^n (p_i)^2 e[k] \right\} \\ &= (1 - \kappa K) e[k] + r[k+1] - r[k] \end{aligned} \tag{9}$$

where

$$\kappa := \sum_i p_i^2. \tag{10}$$

See Remark 1 below for the disturbance response. We evaluate the tracking performance based on this expression and control theory. Firstly, concerning the stability, $e[k]$ remains bounded for any bounded $r[k]$ if and only if $|1 - \kappa K| < 1$, or equivalently

$$0 < K < \frac{2}{\kappa} \tag{11}$$

(see $e[k] = (1-\kappa K)^{k-1} e[0]$ when $r[k]$ is constant). This tells us that K cannot be taken arbitrarily large.

Next, even under this stability condition, $e[k]$ does not necessarily converge to 0. Actually, it follows from frequency response characteristics of linear systems[1] [10] that the error-to-reference ratio at frequency ω is given by $|G_1(e^{\mathbf{i}\omega})|$ with $\mathbf{i} = \sqrt{-1}$ and

$$G_1(z) := \frac{z-1}{z-(1-\kappa K)}. \tag{12}$$

Here, the frequency $\omega \in [0, \pi]$ is defined by the frame. That is, it represents components in the form of $A\sin(\omega k + \theta)$ with real constants A and θ. For example, $\omega = 0$ means static component, and $\omega = \pi$ means a pixel value flips between two different values frame by frame. In the special case where $r[k]$ is constant ($\omega = 0$) as in [20], $e[k]$ converges to 0 because $G_1(e^{\mathbf{i}\cdot 0}) = G_1(1) = 0$ independent of K.

[1] The function $G_1(z)$ is the so-called transfer function from r to e. Straightforwardly applying z-transformation which maps $e[k+m]$ and $r[k+m]$ to $z^m E(z)$ and $z^m R(z)$ respectively, we obtain $E(z) = G_1(z)R(z)$.

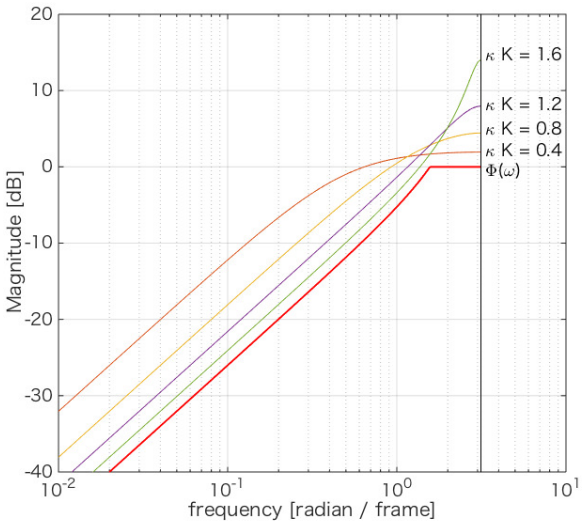

Fig. 4. Frequency dependent error-to-reference ratio and their lower bound.

For general reference moving images $r[k]$, by virtue of the superposition principle, we can expect good precision when $|G_1(e^{i\omega})|$ is small for wide range of ω. See Figure 4 for the plot of $|G_1(e^{i\omega})|$ in decibel for various $K \in (0, 2/\kappa)$. The plot represents the frequency dependent error-to-reference ratio computed as $20\log_{10}(error/reference)$. For example, a projected result of a certain frequency contains an error of 10 % of the reference signal, when the plot takes -20 dB. Note that this figure is independent of κ.

Though Eq. (12) implies that larger K makes $|G_1(e^{i\omega})|$ smaller, Eq. (11) imposes performance limit. Actually, simple calculation yields

$$\sup_{0<K<\frac{2}{\kappa}} \left| e^{i\omega} - (1-\kappa K) \right| = \left| e^{i\omega} + \mathrm{sgn}\left(\frac{\pi}{2} - \omega\right) \right|. \tag{13}$$

Therefore, we obtain the following explicit performance limit

$$\inf_{0<K<\frac{2}{\kappa}} |G_1(e^{i\omega})| = \Phi(\omega) := \left| \frac{e^{i\omega} - 1}{e^{i\omega} + \mathrm{sgn}\left(\frac{\pi}{2} - \omega\right)} \right|, \tag{14}$$

where

$$\mathrm{sgn}(\omega) = \begin{cases} 1, & \omega \geq 0 \\ -1, & \omega < 0 \end{cases} \quad \omega \in \mathbb{R}, \tag{15}$$

The plot of $\Phi(\omega)$ shown in Figure 4 tells us about the previously proposed distributed optimization that error increases with an increment of the frequency, and a projected result contains more than 31.6 % (≈ 10 [dB] $= 1/\sqrt{10}$) of errors at higher frequencies than $\omega = 6 \times 10^{-1}$ even on the lower bound.

4.2 Centralized feedforward mechanism

Figure 5 is a block diagram of the algorithm in the previous section. It is well-known in feedback control theory that tracking responsiveness is difficult to improve by modification of error feedback control parameters. A popular remedy for this is to add *feedforward* mechanism. In what follows, we propose a novel algorithm for movie projection based on this 2-DOF (feedback and feedforward) control design.

We do not change the distributed feedback structure. Let us broadcast the following data in stead of ξ in (5):

$$\xi[k] := K(\underbrace{r[k] - Y[k]}_{e[k]}) + \zeta(r[k+1] - r[k]). \tag{16}$$

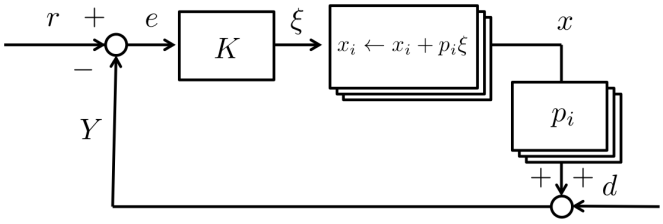

Fig. 5. Block diagram of the distributed gradient method.

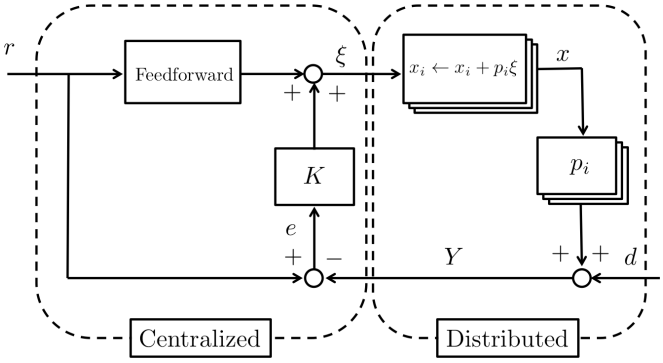

Fig. 6. 2DOF control scheme.

The additional term can be regarded as a centralized feedforward controller with a feedforward gain $\zeta \geq 0$; see Figure 6. Again, this computation should be implemented in the camera node where both reference $r[k]$ and projected result $Y[k]$ are available. Broadcast data size is not increased, that is, it is identical to one frame data.

Next, we investigate when this feedforward mechanism improves the performance. Let us conduct similar analysis as in Subsection 4.1. Direct relationship between $r[k]$ and $e[k]$ is given by

$$\begin{aligned} e[k+1] &= r[k+1] - Y[k+1] \\ &= r[k+1] - \sum_{i=1}^{n} p_i x_i[k+1] \\ &= r[k+1] - \sum_{i=1}^{n} p_i (x_i[k] + p_i \xi[k]) \\ &= r[k+1] - (r[k] - e[k]) \\ &\quad - \kappa\{Ke[k] + \zeta(r[k+1] - r[k])\} \\ &= (1-\kappa K)e[k] + (1-\kappa\zeta)(r[k+1] - r[k]). \end{aligned} \tag{17}$$

This implies the error-to-reference ratio is given by $|G_2(e^{i\omega})|$ with

$$G_2(z) = \frac{(1-\kappa\zeta)(z-1)}{z-(1-\kappa K)} = (1-\kappa\zeta)G_1(z). \tag{18}$$

This means that if we can take

$$\zeta = 1/\kappa, \tag{19}$$

then $G_2(e^{i\omega}) = 0$ for all ω which implies perfect tracking. For other ζ, the performance improvement ratio is independent of ω, and given by

$$\frac{|G_2(e^{i\omega})|}{|G_1(e^{i\omega})|} = |1 - \kappa\zeta|. \tag{20}$$

Remark 1 This additional feedforward mechanism does not change the disturbance rejection characteristics, that is, the response of $e[k]$ to

$d[k]$:

$$\begin{aligned} e[k+1] &= -Y[k+1] \\ &= -d[k+1] - \sum_i^n p_i x_i[k+1] \\ &= -d[k+1] - \sum_i^n p_i \left\{ x_i[k] + K \sum_{i=1}^n p_i e[k] \right\} \\ &= -d[k+1] - (-e[k] - d[k]) - K \sum_{i=1}^n (p_i)^2 e[k] \\ &= (1-\kappa K)e[k] - (d[k+1] - d[k]) \end{aligned} \tag{21}$$

Thus, the error-to-disturbance ratio is

$$G_3(z) = -\frac{z-1}{z-(1-\kappa K)} = -G_1(z) \tag{22}$$

independent of ζ, which is identical to the error-to-reference ratio without feedforward mechanism.

4.3 Robustness to parameter mismatch

Ideally, we could choose ζ using (19) and achieve exact tracking. However, it is impossible to obtain exact value of κ due to measurement errors. In addition, it is desirable from an implementation viewpoint that a common κ is used for all pixels. Hence, in this section, we evaluate the effect of parameter mismatch.

Let us compare $|\Phi(\omega)|$ and $|G_2(e^{i\omega})|$ to see the effectiveness of the proposed scheme. Recall that $G_2(e^{i\omega}) = 0$ for all ω for ζ in (19). We consider the situation with only one projector having the form factor p^j whose histogram is given by Figure 7 (this data was taken from an experiment setting). Considering this distribution and (10), let us regard $\acute{\kappa} = (140/255)^2$ as a nominal value of κ. From Figure 4, let us fix $K = 0.2 \times 2/\acute{\kappa}$. We naturally fix $\zeta = 1/\acute{\kappa}$.

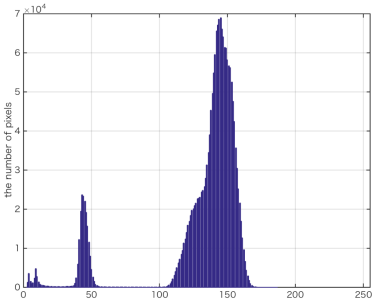

Fig. 7. Histogram of the form factor p^j measured in an experiment setting.

Figure 8 shows $|\Phi(\omega)|$ and $|G_2(e^{i\omega})|$ for p^j's. Figure 9 shows the histogram of the improvement ratio $|1-\kappa^j/\acute{\kappa}|$ in (19) and (20). We can observe that the additional feedforward mechanism significantly improve the tracking performance even for the case where exact value of κ is unavailable. In this case, the error is reduced to 21.9% on avarage.

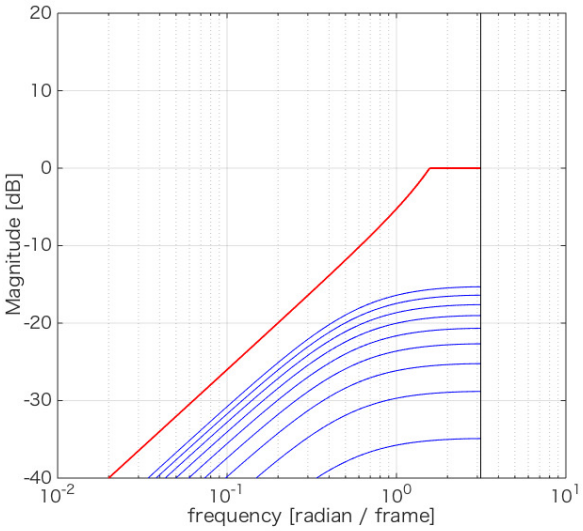

Fig. 8. Error-to-reference ratio improved by the feedforward mechanism.

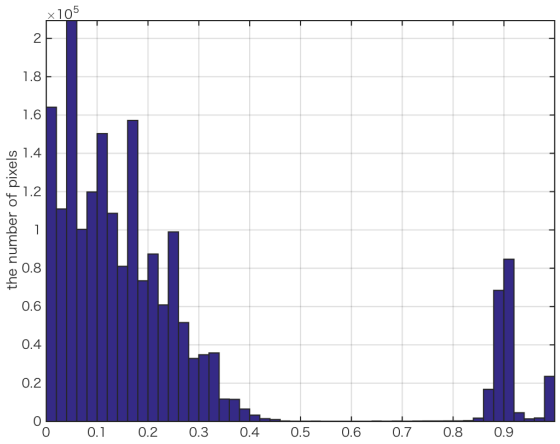

Fig. 9. Histogram of the improvement ratio $|1-\kappa^j/\acute{\kappa}|$ computed at each pixel j. The ratio takes low value (i.e., close to zero) when the improvement of the proposal is high (see (20)).

5 Experiment

We evaluated the proposed technique using a projector-camera system. The system consisted of two projector nodes (EPSON EH-TW410) and a camera node (PointGrey Flea3 FL3-U3-88S2C-C). In the experiment, we virtually built a distributed system by implementing three independent controllers on a PC (CPU: Core-i7-3687U 2.10GHz 2.60GHz, RAM: 8.0GB). The communications among the controllers were limited in such a way that only broadcasting from the camera node to the projector nodes were available. Two projectors were placed so that the two projections were overlapped each other on a target surface. Figure 1 shows the experimental setup.

Figure 10 shows three movie clips from two animation films [4, 9] used as our target images. Each movie clip lasts for around ten seconds under 10 fps (i.e., $k \in [1, 100]$). We call these movies as **animal**, **apple**, and **hand**, respectively. For each movie clip, we prepared a texture that was printed on a sheet of paper, and used as a projection surface (also shown in Figure 10). A cup was placed between the projectors and a target surface as an occluder so that a cast shadow was removed by two overlapping projections. Specifically, one of the projectors is occluded while the other is not. We call the occluded one as projector 1, and the other as projector 2 in the following manuscript.

We used a graycode patten projection technique to acquire pixel correspondences between the camera and each projector [18]. Uniform white images were then projected to acquire the form factors p, as shown in the third and forth rows of Figure 10. These geometric and colorimetric calibrations were performed once in advance.

5.1 Conditions and Results

To evaluate how the proposed technique improves the tracking responsiveness over the previous feedback-only approach, we prepared three experimental conditions for each target movie clip. In the first condition, the proposed 2-DOF control technique was applied to compensate for the target images. The previous feedback-only technique was applied in the second and third conditions. The parameter K in the second condition was set as the same value with the first condition. We experimentally decided the parameters K and ζ (only for the 2-

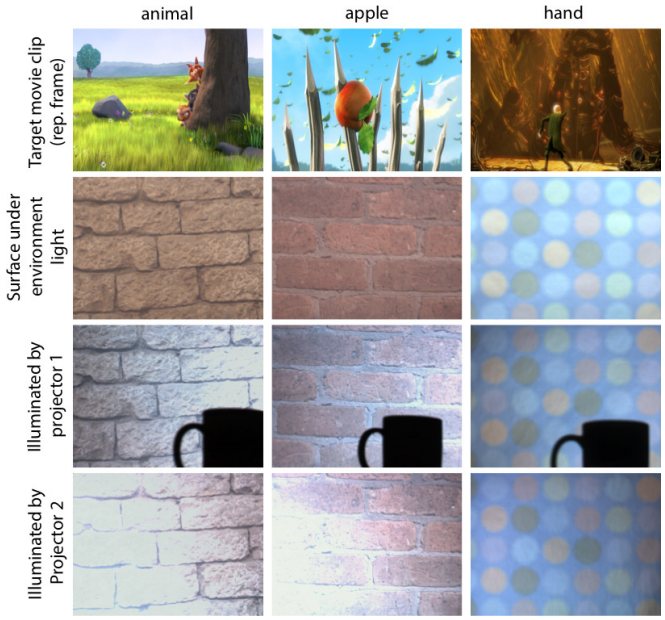

Fig. 10. Target movie clips and projection surfaces: (top row) a representative frame of target movie clip, (second row) the appearance of projection surface under environment light, (third row) the surface under uniform white illumination by projector 1, and (fourth row) that by projector 2.

Target movie	Condition	K	ζ
animal	2-DOF	0.5	1.3
	Feedback-only	0.5	n/a
	Feedback-only (larger K)	1.3	n/a
apple	2-DOF	0.5	1.5
	Feedback-only	0.5	n/a
	Feedback-only (larger K)	1.8	n/a
hand	2-DOF	1.5	2.0
	Feedback-only	1.5	n/a
	Feedback-only (larger K)	3.8	n/a

Table 1. Parameters.

DOF condition) from initial values given by the method described in Section 4.3. Note that we used common parameters for all pixels and frames. In the third condition, we set a larger K, because generally a larger gain provides a feedback system with a quicker convergence. We experimentally decided the larger K within the bound of (11) as it successfully compensated for regions of target images showing large temporal variations, such as those showing animals. Table 1 shows the parameters in each condition.

Furthermore, to evaluate the robustness and scalability of the proposed technique, we conducted experiments under three additional conditions. We prepared the first one for a plug-in situation where a projector node was newly added to the system. The second one is for an opposite situation where a projector node connected to the system was suddenly stopped. We prepared the last condition to validate the robustness of the proposed technique for disturbance such as the sudden change of environment light. In the above three conditions, each event happened at the 21-st frame of a movie. The same parameters with the 2-DOF condition were applied in these conditions. In total, we prepared six experimental conditions.

We conducted eighteen projection experiments (=three target movie clips×six conditions). As an example of projected results, Figure 1 shows the target image r, the broadcasted data ξ, the input images x_i, and the projected result Y at the 76-th frame of the animal movie under 2-DOF condition. Note that the projection results of whole image sequences are shown in our supplementary material. We evaluated the image qualities of projected results using the structural similarity index (SSIM) [22], which is a method for assessing the perceptual quality of a distorted image when compared to the original. The time series of SSIM values are shown in Figure 11 for the comparison among the 2-DOF and feedback-only conditions, and in Figure 16 for evaluation of robustness of the proposed 2-DOF control method.

5.2 Discussion on Time Responsiveness

Here, we discuss on the improvement of time responsiveness by the proposed 2-DOF control approach by comparing the results among three conditions, 2-DOF, feedback-only, and feedback-only with larger K. In the SSIM values in Figure 11, it can be seen that 2-DOF provides the best image quality at most of the frames.

Figure 12 shows the time series of target images and projected results of the animal movie under the three conditions. First, we can observe in the third row that quickly moving animals almost disappear in some frames in the feedback-only case with $K = 0.5$. This means that the previous method with lower gain K could not properly compensate for image regions where target images showed large temporal variations, which got strongly blurred. This is a consequence of the lack of responsiveness. Next, as in the forth row, this point is improved by choosing larger gain K. However, it causes *flickering* in particular after 60-th frame. This is a consequence of the large tracking error observed around the highest frequency in Figure 4 for large K's. This unstable behaviour for large K is obvious in SSIM values in Figure 11. On the other hand, the results in the second row solved these two issues simultaneously. From the results, we confirmed that the proposed 2-DOF control provided the best compensation results among all methods.

In addition, to see more in details how the proposed technique worked, we show the broadcasted data ξ at the 26-th frame of 2-DOF and feedback-only conditions in Figure 13. As shown in the figure, the broadcasted data of the 2-DOF control method contains both the current and next frames information, while that of the feedback-only method only contains the current frame information. Actually, the additional term in (16) is the difference between two consecutive frames. Therefore, this component provides information about the direction of the movement contained in the target images, somewhat like optical flows. This can be viewed as a reason that the broadcasted data takes higher values around the boundary of the moving objects.

5.3 Discussion on Robustness

We discuss how the proposed technique is robust for system state changes due to the following three factors: plug-in, plug-out, and disturbance. The first and second rows of Figure 14 show the selected target images from the apple movie, and the corresponding projected results where a new projector was plugged in at the 21-th frame. From the first to the 20-th frame, there was a shadow of the cup where no image could be projected by a single projector. The texture of the projection surface was also visible in the non-shadowed area due to the limited maximum intensity of the projector. At the 21-st frame when the other projector was added to the system, the projected result was oversaturated because the system computed the input image to each projector based on the previous projected result which was darker than the target image. But ten frames later, the compensation worked without saturations. This feature can be seen in the SSIM values (dashed blue line in Figure 16) of all three movies. We confirmed that the proposed technique performed radiometric compensation under a plug-in situation.

The lowest column of Figure 14 shows the projected results of the apple movie under the plug-out condition where one of the projectors stopped at the 21-th frame. From the first to the 20-th frame, the projected results were compensated well. At the 21-st frame when a projector whose projected image was occluded by the cup was stopped, the projected result became darker except for the cup shadow area on which only a non-occluded projector displayed images in the previous frames. Ten frames later, such inconsistency was solved but the texture of the projection surface became visible due to the limited maximum intensity of the projector. This feature can be seen in the SSIM values

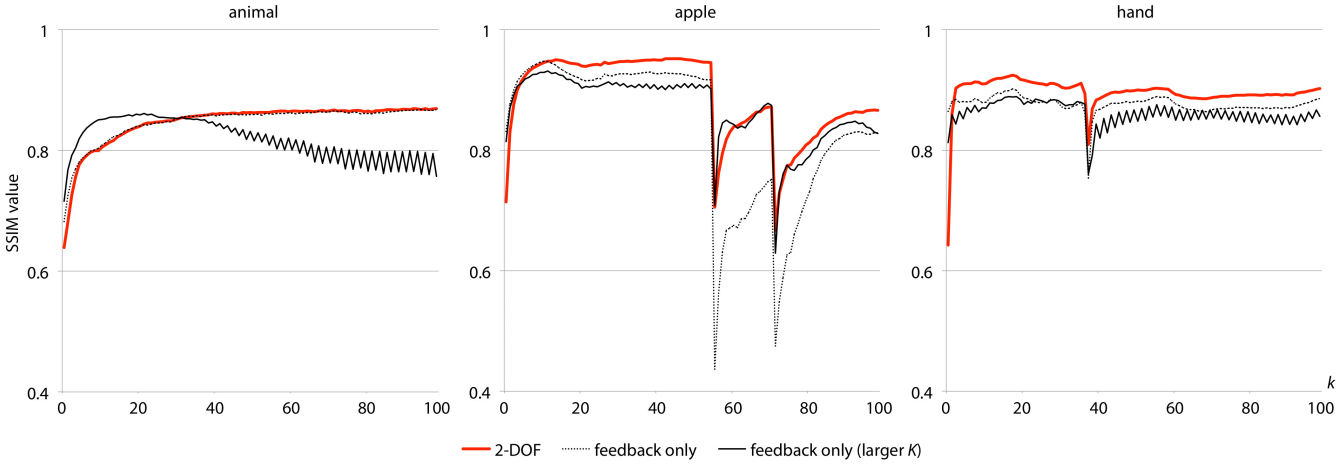

Fig. 11. Time series of SSIM values: (left) **animal**, (middle) **apple**, and (right) **hand**.

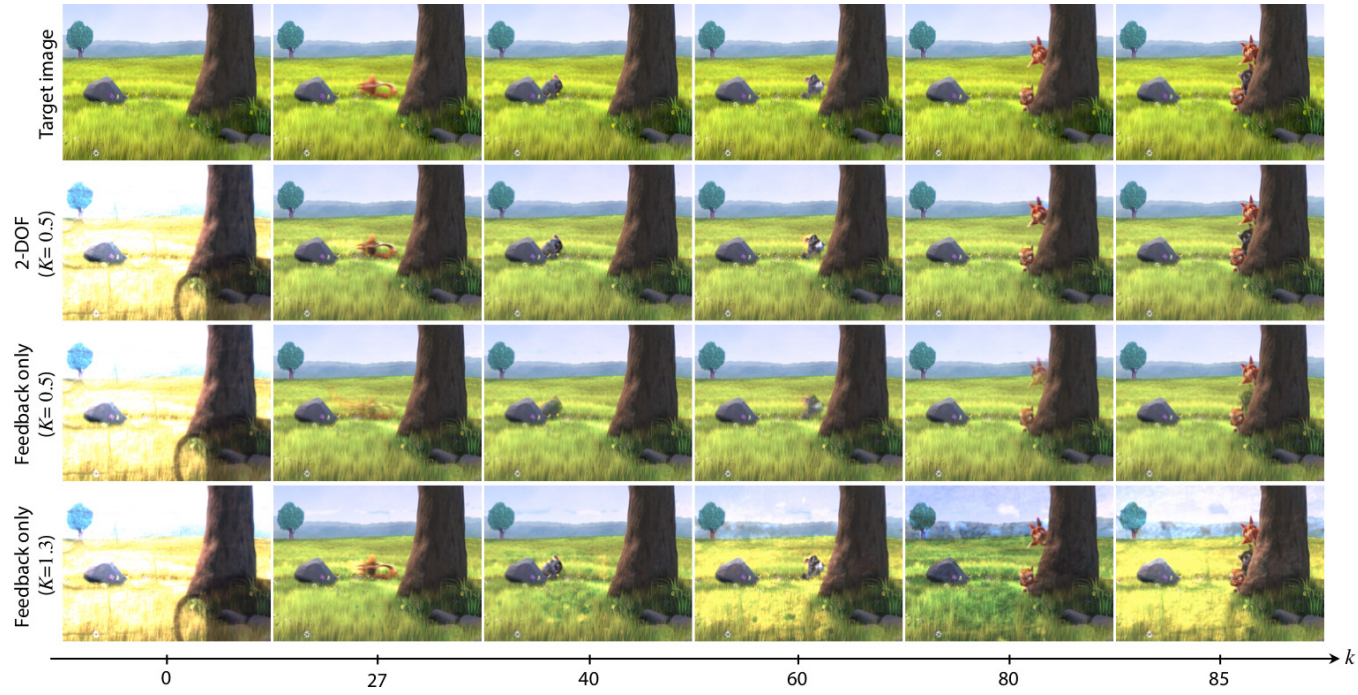

Fig. 12. Movie clips of the target and projection results: (top row) representative frames of target movie clip, (second row) the results by the proposed 2-DOF control method, (third row) the results by the feedback-only method, (forth row) the results by the feedback-only method with a higher gain K.

(solid blue line in Figure 16) of all three movies. We confirmed that the proposed technique properly performed radiometric compensation under a plug-out situation.

Figure 15(a) shows the time series of target images and projected results of the hand movie under the disturbance condition where a ceiling light was turned on at the 21-th frame. From the first to the 20-th frame, the projected results were well compensated. The projected result became a little bit brighter due to the disturbance at the 21-st frame, while the projected results were well compensated again only a couple of frames later. A side-by-side comparison is provided in Figure 15(b) to see the slight brightness difference. This feature can be seen in the SSIM values (solid green line in Figure 16) of all three movies. In the SSIM results of animal and hand movies, we can also see that the compensation performance did not reach to the upper bound (i.e., that of 2-DOF condition) due to the increment of the black offset by the additional environment light. We confirmed that the proposed technique performed radiometric compensation under a disturbance situation.

6 Limitation

The system is not able to adapt for geometrical changes of the projection surface. We assume that all distributed projectors are geometrically registered for the screen surface in advance. This might be a problem if a user wish to add a plug-in projector, because such additional projector can be placed at an arbitrary position. In this case, on-line geometrical registration is required. One solution is to apply an imperceptible calibration method [24] to the system such that a newly added projector projects graycode pattern images which are detected only by a camera for geometric calibration, while human observers do not perceive them. This would be an interesting future direction of this research.

The proposed algorithm assumes perfect synchronization between camera and projectors. However, in theory, it also converges without synchronization while the frame rates of camera and projectors are

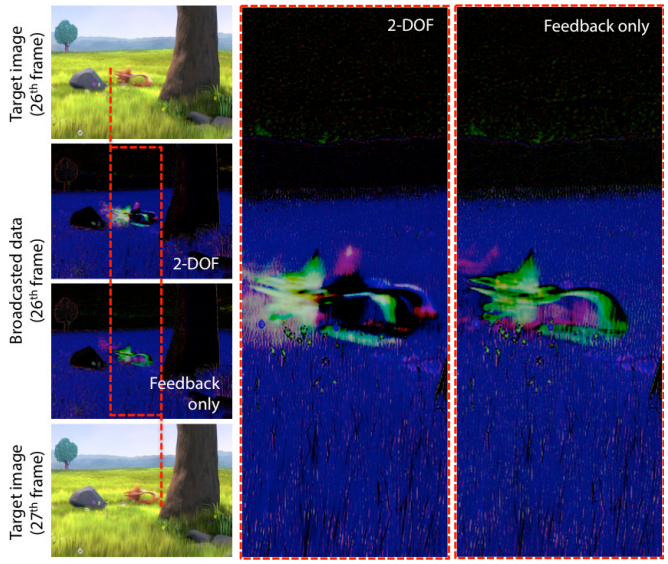

Fig. 13. Broadcast data: (left) target image and broadcasted data at 26-th and 27-th frame, (middle) enlarged broadcasted data by the proposed 2-DOF control method, (right) enlarged broadcasted data by the feedback-only method.

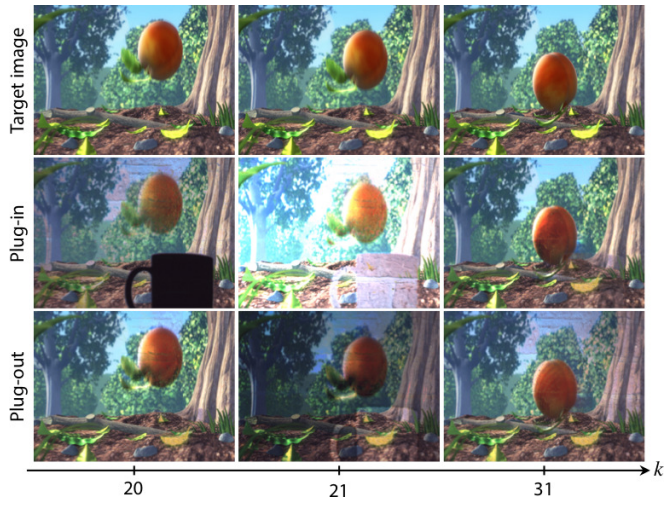

Fig. 14. Movie clips for robustness evaluation: (top row) the target images, (second row) plug-in results, (third row) plug-out results.

identical. In such case, the tracking responsiveness is still improved compared to the feedback-only method, but becomes worse than the 2-DOF control method.

In the proposed algorithm, synchronization between the camera and the projectors is not significant. Actually, almost the same performance can be guaranteed theoretically as long as each projector updates their projection image before the camera observation at the next frame. However, the performance degradation caused by longer delays (e.g., by signal processing, information transfer) should be carefully evaluated.

The current implementation is not optimized and too slow for a real-time processing (1 fps). As with many previous radiometric compensation techniques, it can be easily parallelized and implemented on GPU to run in real-time.

7 Conclusion

In this paper, we proposed a novel radiometric compensation technique for cooperative projection system. Its important feature is that

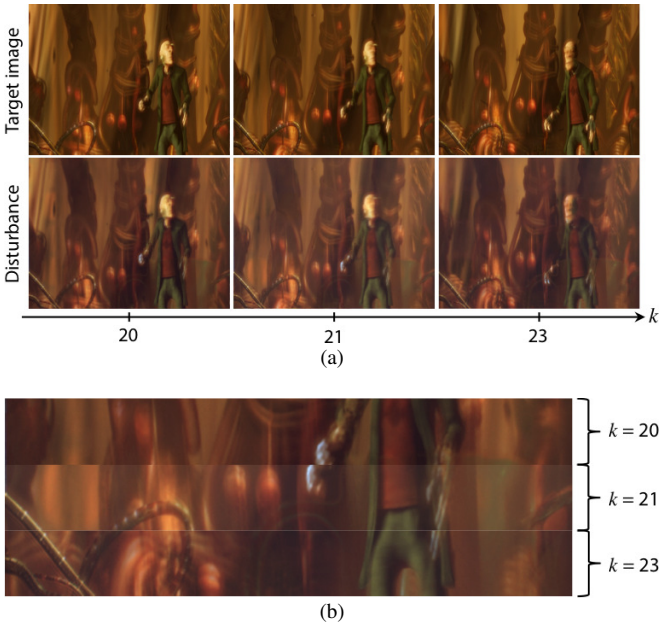

Fig. 15. Movie clips for environmental light adaptation (a): (first row) the target images and (second row) the projection results under the change of the ceiling light. Projection results for a region just before and after the change of ceiling light are shown in (b).

we constructed a 2 Degree Of Freedom control structure. More specifically, this system consists of two algorithms: 1. decentralized projection image update based on the distributed gradient method implemented at each projector, and 2. centralized error image broadcast implemented at the camera node. While the former is crucial to attain scalability and robustness only via limited information exchange, the latter significantly improves the responsiveness to enable the moving image projection with an high accuracy. The effectiveness was quantitatively guaranteed by the mathematical analysis of the error-to-reference ratio. Also, real projection experiments based on the proposed method were demonstrated.

Since this is the first step to apply control theoretic technique to develop cooperative projection system, there are many interesting and also challenging problems. Processing delays in the feedback loop, adaptive/learning mechanism, spatio-temporal frequency analysis are promising direction for system design for better cooperative projection systems, and are currently under investigation.

Acknowledgments

Thanks to Yuki Minai for valuable discussions. This research was supported by JSPS KAKENHI Grant Number 26630198.

References

[1] T. Amano and H. Kato. Appearance control using projection with model predictive control. In *Proceedings of International Conference on Pattern Recognition (ICPR)*, pages 2832–2835, 2010.

[2] T. Amano, I. Shimana, S. Ushida, and K. Kono. Successive wide viewing angle appearance manipulation with dual projector camera systems. In *Proceedings of International Conference on Artificial Reality and Telexistence and Eurographics Symposium on Virtual Environments (ICAT-EGVE)*, pages 49–54, 2014.

[3] A. Bermano, P. Brüschweiler, A. Grundhöfer, D. Iwai, B. Bickel, and M. Gross. Augmenting Physical Avatars Using Projector Based Illumination. *ACM Transactions on Graphics*, 32(6):189:1–189:10, 2013.

[4] Big Buck Bunny. https://peach.blender.org/, 2015.

[5] O. Bimber and A. Emmerling. Multi-focal projection: A multi-projector technique for increasing focal depth. *IEEE Transactions on Visualization and Computer Graphics*, 12(4):658–667, 2006.

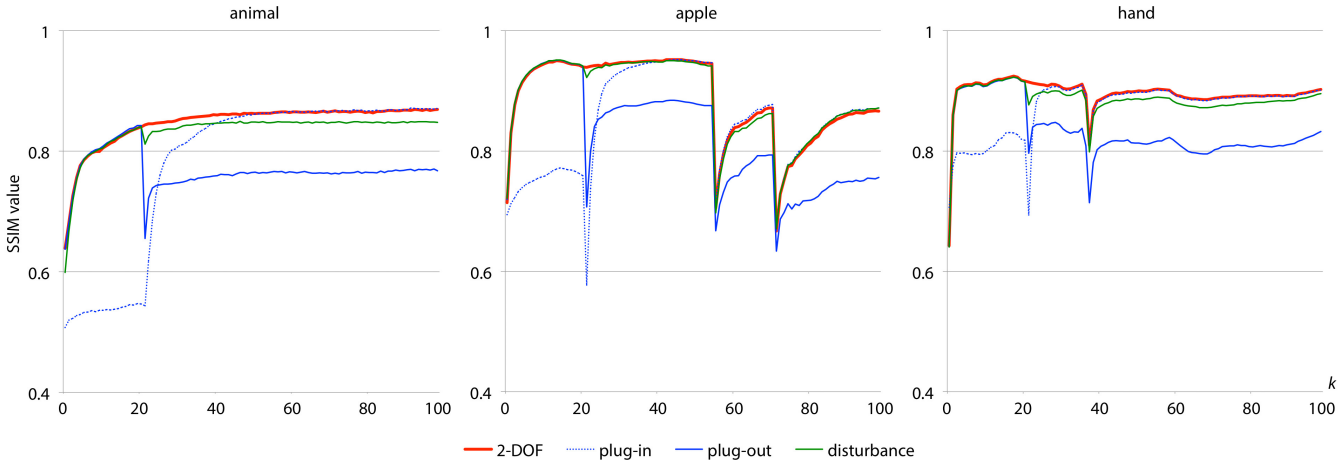

Fig. 16. Time series of SSIM values: (left) **animal**, (middle) **apple**, and (right) **hand**.

[6] O. Bimber, A. Emmerling, and T. Klemmer. Embedded entertainment with smart projectors. *IEEE Computer*, 38(1):56–63, 2005.
[7] O. Bimber, D. Iwai, G. Wetzstein, and A. Grundhöfer. The Visual Computing of Projector-Camera Systems. *Computer Graphics Forum*, 27(8):2219–2254, 2008.
[8] F. Bullo, J. Cortes, and S. Martinez. *Distributed Control of Robotic Networks:A Mathematical Approach to Motion Coordination Algorithms*. Princeton Series in Applied Mathmatics, 2009.
[9] Elephants Dream. https://orange.blender.org/, 2015.
[10] G. F. Franklin, J. D. Powell, and M. L. Workman. *Digital Control of Dynamic System*. Addison-Weley, 2nd edition, 1990.
[11] L. Itti and C. Koch. Computational modeling of visual attention. *Nature Reviews Neuroscience*, 2(3):194–203, 2001.
[12] D. Iwai, M. Nagase, and K. Sato. Shadow removal of projected imagery by occluder shape measurement in a multiple overlapping projection system. *Virtual Reality*, 18(4):245–254, 2014.
[13] M. Mesbahi and M. Egerstedt. *Graph Theoretic Methods in Multiagent Networks*. Princeton Series in Applied Mathmatics, 2010.
[14] S. Mihara, D. Iwai, and K. Sato. Artifact reduction in radiometric compensation of projector-camera systems for steep reflectance variations. *IEEE Transactions on Circuits and Systems for Video Technology*, 24(9):1631–1638, 2014.
[15] M. Nagase, D. Iwai, and K. Sato. Dynamic defocus and occlusion compensation of projected imagery by model-based optimal projector selection in multi-projection environment. *Virtual Reality*, 15(2):119–132, 2011.
[16] A. Nedic and A. Ozdaglar. Distributed Subgradient Method for Multi-agent Optimization. *IEEE Transactions on Automatic Control*, 54(1):48–61, 2009.
[17] M. Ramasubramanian, S. N. Pattanaik, and D. P. Greenberg. A perceptually based physical error metric for realistic image synthesis. In *Proceedings of SIGGRAPH*, pages 73–82, 1999.
[18] K. Sato and S. Inokuchi. Range-Imaging System Utilizing Nematic Liquid Crystal Mask. In *Proceedings of IEEE International Conference on Computer Vision (ICCV)*, pages 657–661, 1987.
[19] Stephen Boyd. http://www.stanford.edu/class/ee364b/lectures/subgrad_method_notes.pdf, 2015.
[20] J. Tsukamoto, D. Iwai, and K. Kashima. Radiometric compensation of cooperative projection system based on distributed optimization. *Transactions of Virtual Reality Society Japan*. under review. in Japanese.
[21] D. Wang, I. Sato, T. Okabe, and Y. Sato. Radiometric compensation in a projector-camera system based on the properties of human vision system. In *Proceedings of IEEE International Workshop on Projector-Camera Systems*, 2005.
[22] Z. Wang, A. C. Bovik, H. R. Sheikh, and E. P. Simoncelli. Image quality assessment: From error visibility to structural similarity. *IEEE Transactions on Image Processing*, 13(4):600–612, 2004.
[23] T. Yoshida, C. Horii, and K. Sato. A virtual color reconstruction system for real heritage with light projection. In *Proceedings of International Conference on Virtual Systems and Multimedia*, pages 161–168, 2003.
[24] S. Zollmann and O. Bimber. Imperceptible calibration for radiometric compensation. In *Proceedings of Eurographics*, pages 61–64, 2007.